Journal of Photochemistry and Photobiology A: Chemistry 276 (2013) 104–112

Contents lists available at ScienceDirect

Journal of Photochemistry and Photobiology A: Chemistry

journal homepage: www.elsevier.com/locate/jphotochem

Synthesis and characterization of free base and metal porphyrins and their interaction with CdTe QDs

S. Jagadeeswari, G. Paramaguru, R. Renganathan*

School of Chemistry, Bharathidasan University, Tiruchirappalli 620 024, Tamil Nadu, India

ARTICLE INFO

Article history:
Received 18 August 2013
Received in revised form
11 November 2013
Accepted 18 November 2013
Available online 12 December 2013

Keywords:
Quantum dots
Free base porphyrins
Metalloporphyrins
Electron transfer
Transient absorption measurements
Photoluminescence quenching

ABSTRACT

Free base porphyrins and metalloporphyrins with different number of methoxy groups were synthesized to investigate the consequence of methoxy groups in the porphyrins on interaction with quantum dots through steady state, time resolved and transient absorption measurements. Spectral changes in the absorption and photoluminescence of quantum dots in the presence of porphyrins elucidate the binding affinity between them. From the photoluminescence quenching analysis, higher number of methoxy substituted zinc porphyrin was found to possess better binding affinity with quantum dots than the other porphyrins which divulges the role of methoxy substituents. The calculated reduction potential of the synthesized porphyrins was feasible for accepting electrons from the photoexcited quantum dots. Electron transfer mechanism is suggested based on energy level diagram, Rehm–Weller equation and transient absorption measurements.

1. Introduction

Quantum dots (QDs) have received great attention in various fields such as photovoltaic and biological applications [1–6]. Among these potential applications, quantum dot sensitized solar cells (QDSSC) is currently of great interest due to their unique properties such as quantum confinement effect [7], larger extinction coefficient [8], multiple excition generation [9], narrow emission bands with broad absorption wavelength, photostability, etc. However, the photocurrent efficiency of QDSSC is very low due to difficulty of assembling a sufficiently large number of QDs on a mesoporous TiO_2 matrix in order to obtain a well-covered monolayer without cluster formation [7] and also the presence of surface states possessing both electron and hole traps in the QDs, which results in lower short circuit current and open-circuit photovoltage [10,11]. The retardation of blocking of the surface states was achieved through the surface passivation of QDs by using ZnS [12], amorphous TiO_2 layer [13], dyes [14], etc. Surface passivation of QDs and organic dye molecules results in a class of new materials which will be important for photovoltaics [15]. The electron accepting properties of organic compounds have been utilized for photocurrent generation, and thus to improve the capture of photogenerated electrons from QDs [16].

Porphyrin is a macrocyclic molecule with unique photophysical and electrochemical properties. The optoelectronic properties of the porphyrins were tuned by varying the meso-functional ligands and metal insertion sites [13]. For electron transfer to occur the potential values of the QDs and Porphyrins should be favorable and they should possess efficient binding between them. The electron transfer from QDs to organic photosensitizers was evidenced by transient absorption measurements in literature [17,18]. Recently, Patra et al. utilized the QDs–porphyrin systems as optical-based sensor for bio applications [18]. Borczyskowski et al. have widely analyzed the photophysical properties of QDs with porphyrin systems [19]. Based on this, the effect of methoxy substituted free base (Pn1, Pn2 and Pn3) and metal porphyrins (ZnPn1, ZnPn2 and ZnPn3) (Scheme 1) on interaction with thioglycolic acid stabilized CdTe QDs were probed by using steady state, time resolved and transient absorption measurements.

2. Experimental

2.1. Materials

Thioglycolic acid (TA), $CdCl_2{\cdot}2.5H_2O$ (99.99%), tellurium powder (99.997%), sodium borohydride (95%), syringaldehyde (>98%), pyrrole (98%) and tetra butyl ammonium hexafluoro phosphate were purchased from Sigma–Aldrich. 4-Hydroxy benzaldehyde and solvents were of analytical grade purchased from LOBA Chemicals (India). Vanillin, propionic acid and $Zn(OAc)_2{\cdot}2H_2O$ were

* Corresponding author. Tel.: +91 431 2407053; fax: +91 431 2407045.
E-mail address: rrengas@gmail.com (R. Renganathan).

1010-6030/$ – see front matter © 2013 Elsevier B.V. All rights reserved.
http://dx.doi.org/10.1016/j.jphotochem.2013.11.018

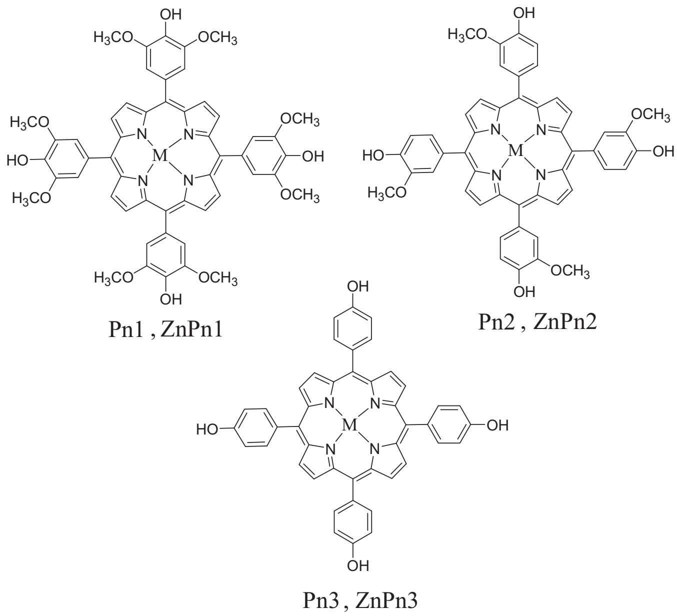

M = 2H **(Pn1, Pn2, Pn3)**
Zn^{2+} **(ZnPn1, ZnPn2, ZnPn3)**

Scheme 1. Structures of porphyrins and metalloporphyrins.

obtained from Merck chemicals. Double distilled water was used for preparing solutions. All measurements were performed at ambient temperature. CdTe quantum dots were synthesized by using the following method as reported earlier [20]. The quantum yield of prepared QDs was 15%, calculated using rhodamine B as the reference.

2.2. Instrumentation

Absorption measurements were recorded using JASCO V630 UV–visible spectrophotometer. Photoluminescence (PL) measurements were carried out using Perkin Elmer LS 55 spectrofluorimeter. The excitation and emission wavelength of TA-CdTe QDs were 500 and 595 nm, respectively. Silt width (10 nm) and scan rate (200 nm/min) were kept constant for all measurements. Quartz cells (4 × 1 × 1 cm) with high vacuum Teflon stopcocks were used for measurements. Samples for absorption and photoluminescence measurements were prepared by adding various concentration [0–5 × 10^{-5} M] of porphyrins to the test tubes containing QDs [1 × 10^{-6} M] and then kept as such for 1 h and used for further experiments. Cyclic voltammogram was acquired with Princeton EG and G-PARC model potentiostat using Glassy carbon working electrode, Ag/AgCl reference electrode and platinum wire counter electrode. Tetrabutyl ammonium hexafluoro phosphate (0.1 M) was used as supporting electrolyte for porphyrins/metalloporphyrins in DMF solvent. All samples were deaerated by bubbling with nitrogen gas for ca.5 min at room temperature. ^{1}H NMR and ^{13}C NMR spectrum were obtained using a Bruker spectrometer (400 MHz). FT-IR spectra were obtained by using Perkin–Elmer Spectrum RXI FT-IR Spectrometer at room temperature in the range of 4000–400 cm^{-1}.

PL lifetime measurements were carried out in a picosecond time correlated single photon counting (TCSPC) spectrometer. The excitation source was the tunable Ti-sapphire laser (TSUNAMI, Spectra Physics, USA). The data analysis was carried out by the software provided by IBH (DAS-6). For Laser Flash Photolysis measurements, the Nd–YAG laser source produces nanosecond pulses (8 ns) of 532 nm light and energy of the laser pulse was around 150 mJ. Dichroic mirrors were used to separate the third harmonic from the second harmonic and the fundamental output of the Nd–YAG laser. The monitoring source was a 150 W pulsed xenon lamp which was focused on the sample at 90° to the incident laser beam. The beam emerging through the sample was focused onto a Czerny–Turner monochromator using a pair of lenses. The detection was carried out using a Hamamatsu R-928 photomultiplier tube. The transient signals were captured with an Agilent infiniium digital storage oscilloscope interfaced to a computer.

2.3. General synthesis of free base porphyrins and metalloporphyrins

Corresponding aldehyde precursors (5.4 mmol) was dissolved in propionic acid (54.65) and the solution was heated to 140 °C. A freshly distilled pyrrole (5.4 mmol) was slowly added and refluxed for 1 h. Under hot condition 55 ml of anhydrous alcohol was added and the solution was transferred into beaker cooled to room temperature and kept 1 h at −5 °C. Filtered the solution to obtain blue powder and dried. A solution of $Zn(OAc)_2{\cdot}2H_2O$ (2 mol) in ethanol (1 ml) was added to the solution of free base porphyrins (1 mol) in $CHCl_3$ and stirred overnight at room temperatureunder N_2 in the dark. This was monitored by TLC and the mixture was washed with water and evaporated to dryness to get desired compound.

2.3.1. Meso-tetrakis (4-hydroxy-3,5-dimethoxy phenyl) porphyrin (Pn1)

Yield – 4.23%, color: glittering purple color, ^{1}H NMR (400 MHz, DMSO): δ (ppm), 8.92 (s, 8H, β pyrrole), 7.45 (s, 8H, 2,6-phenyl), 3.88 (s, 24H, —OCH3), −2.47 (s, 2H, NH-pyrrole), 8.86 (s, 4H, —OH). ^{13}C NMR (400 MHz, DMSO): 146.35, 135.61, 131.37, 120.86, 112.86, 56.27. IR (KBr, cm^{-1}): 3464, 2929, 1603, 1509, 1453, 1411, 1341, 921, 800, 730 cm^{-1}. MS (MALDI) *m*/*z* calculated for $C_{52}H_{46}N_4O_{12}$ (M+H): 918.31, Found: 919.23.

2.3.2. Meso-tetrakis (4-hydroxy-3-methoxy phenyl) porphyrin (Pn2)

Yield – 8.1%, color: purple powder, ^{1}H NMR (400 MHz, DMSO): δ (ppm), 9.51 (s, 4H, —OH), 8.9 (s, 8H, β pyrrole), 7.76 (s, 4H, 2-phenyl), 7.58-7.57 (d, 4H, 6-phenyl), 7.1-7.2 (d, 4H, 5-phenyl), 3.89 (s, 12H, —OCH3) −2.88 (s, 2H, NH-pyrrole).). ^{13}C NMR (400 MHz, DMSO): 146.63, 146.01, 132.34, 127.48, 120.03, 118.89, 114.03, 55.85. FT-IR (KBr, cm^{-1}): 3492, 3427, 2929, 1603, 1509, 1463, 1416, 1341, 1229, 1262, 1117, 1033, 916, 865, 730 cm^{-1}. MS (MALDI) *m*/*z* calculated for $C_{48}H_{38}N_4O_8$ (M+H): 798.27, Found: 799.02.

2.3.3. Meso-tetrakis (4-hydroxy phenyl) porphyrin (Pn3)

Yield – 3.1%, color: glittering green color, ^{1}H NMR (400 MHz, DMSO): δ (ppm), 9.96 (s, 4H, —OH), 8.86 (s, 8H, β pyrrole), 7.9-8 (d, 8H, 2,6-phenyl), 7.1-7.2 (d, 8H, 3,5-phenyl), −2.89 (s, 2H, NH-pyrrole). ^{13}C NMR (400 MHz, DMSO): 157.37, 135.49, 131.90, 119.97, 113.90. IR (KBr, cm^{-1}): 3412, 3220, 1509, 1603, 1478, 1379, 1279, 1171, 1112, 846 cm^{-1}. MS (MALDI) *m*/*z* calculated for $C_{44}H_{30}N_4O_4$(M+H): 678.23, Found: 679.016.

2.3.4. Zn(II)-[meso-tetrakis (4-hydroxy-3,5-dimethoxy phenyl) porphyrin] (ZnPn1)

Yield – 68%, color: blue solid, ^{1}H NMR (400 MHz, DMSO): δ (ppm), 8.92 (s, 8H, β pyrrole), 7.45 (s, 8H, 2,6-phenyl), 3.88 (s, 24H, —OCH3), 8.86 (s, 4H, —OH).). ^{13}C NMR (400 MHz, DMSO): 149.53, 146.07, 135.22, 132.95, 131.49, 120.39, 112.82, 56.25. IR (KBr, cm^{-1}): 3464, 2929, 2845, 1607, 1509, 1453, 1411, 1341, 1206, 1114, 940, 795 cm^{-1}. MS (MALDI) *m*/*z* calculated for $C_{52}H_{44}N_4O_{12}Zn$ (M^+): 980.22, Found: 979.85.

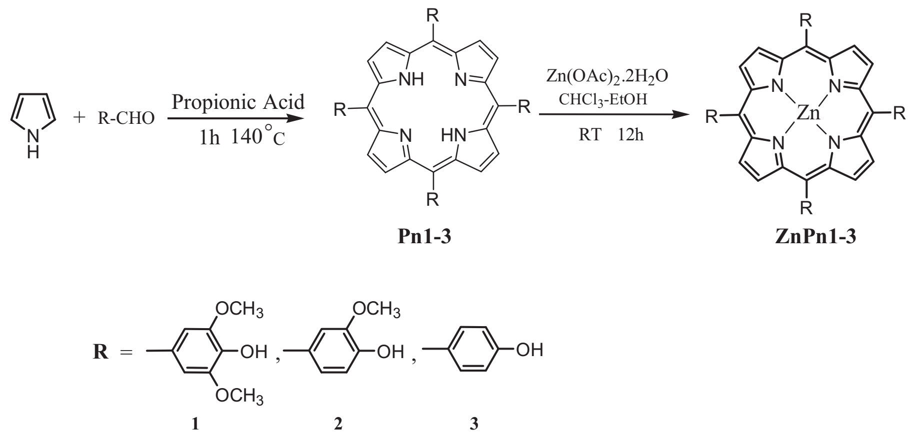

Scheme 2. Synthesis of porphyrins and metalloporphyrins.

2.3.5. *Zn(II)-[meso-tetrakis (4-hydroxy-3-methoxy phenyl) porphyrin] (ZnPn2)*

Yield – 74%, color: black powder, ^{1}H NMR (400 MHz, DMSO): δ (ppm), 9.51 (s, 4H, —OH), 8.9 (s, 8H, β pyrrole), 7.76 (s, 4H, 2-phenyl), 7.58-7.57 (d, 4H, 6-phenyl), 7.1-7.2 (d, 4H, 5-phenyl), 3.89 (s, 12H, —OCH3). ^{13}C NMR (400 MHz, DMSO): 149.57, 146.14, 145.65, 133.91, 131.44, 127.33, 120.27, 118.87, 113.70, 55.83. IR (KBr, cm^{-1}): 3437, 2929, 2845, 1593, 1509, 1458, 1332, 1239, 1159, 1033, 996,776 cm^{-1}. MS (MALDI) m/z calculated for $C_{48}H_{36}N_4O_8Zn$ (M^+): 860.18, Found: 860.13.

2.3.6. *Zn(II)-[meso-tetrakis (4-hydroxy phenyl) porphyrin] (ZnPn3)*

Yield – 55%, color: blue powder, ^{1}H NMR (400 MHz, DMSO): δ (ppm), 9.96 (s, 4H, —OH), 8.86 (s, 8H, β pyrrole), 7.9-8 (d, 8H, 2,6-phenyl), 7.1-7.2 (d, 8H, 3,5-phenyl). ^{13}C NMR (400 MHz, DMSO): 156.85, 149.58, 135.25, 133.45, 131.37, 120.21, 118.55, 113.47. IR (KBr, cm^{-1}): 3417, 1607, 1509, 1425, 1337, 1210, 1170, 1098, 996, 800 cm^{-1}. MS (MALDI) *m/z* calculated for $C_{44}H_{28}N_4O_4Zn$ (M^+): 740.14, Found: 740.15.

3. Results and discussion

3.1. *Synthesis and characterization of porphyrins and metalloporphyrins*

Free base porphyrins and metalloporphyrins were synthesized according to the literature procedure [21,22]. Free base porphyrins were prepared by the condensation of aldehydes with pyrrole in the presence of propionic acid (Scheme 2). A metallation of free base porphyrins with zinc acetate dihydrate leads to the formation of metalloporphyrins. The synthesized P/MP was successfully characterized by ^{1}H and ^{13}C NMR, Mass, IR, UV–Vis absorbance and PL measurements. Experimental procedure and spectral data were given in supporting information.

Free base porphyrins showed a characteristic broad singlet peak at −2.873 ppm (Pn1), −2.88 ppm (Pn2) and −2.889 ppm (Pn3), which are assigned to NH proton in porphyrin ring. NH peak of pyrrole unit disappeared after the insertion of Zn(II) dication into free base porphyrins (Scheme 3). The quantum yields of P/MP in DMF are shown in Table 1, calculated using TPP as a standard.

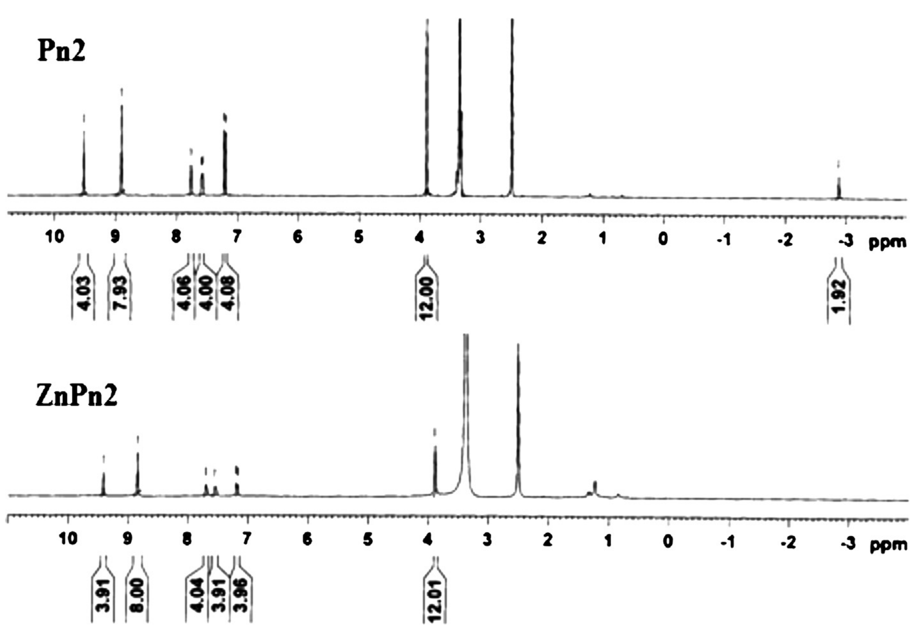

Scheme 3. ^{1}H NMR spectrum of Pn2 (free base porphyrin) and ZnPn2 (metalloporphyrin).

Table 1
Optical and electrochemical parameters of P/MP.

P/MP	λ_{abs} (nm)		λ_{em} (nm)	$E_{1/2}^{(red)}$ (V)	QY
	Soret band	Q band			
Pn1	428	517, 556, 592, 649	672	−1.104	0.101
Pn2	426	514, 551, 591, 646	673	−1.071	0.107
Pn3	423	512, 550, 588, 646	673	−1.049	0.103
ZnPn1	432	557, 598	627, 675	−1.252	0.099
ZnPn2	431	556, 598	628, 674	−1.128	0.138
ZnPn3	429	557, 598	628, 673	−1.083	0.111

3.1.1. Optical properties

Generally P/MP exhibit two distinct visible absorption regions. The most intense absorption band, commonly referred to as Soret band, exists in the 400-440 nm region. The free base porphyrins possess four absorption bands (Q bands) in the 500-650 nm region. Q bands of metallated porphyrins exhibit two absorptions in this region, due to increase in porphyrins symmetry. Fig. 1A and B shows the absorption and emission spectrum of the synthesized P/MP. Strong Soret bands in the higher energy region and Q bands in the lower energy region are observed for P/MP. The absorption of metallated porphyirns (ZnPn1–3) is notably red-shifted from those of free base porphyrins (Pn1–3) (Insets shows Soret band). Due to metallation, electronic coupling (conjugation) between electron rich methoxy substituted phenyl rings and metal porphyrin unit increases and results in decrease in energy gap (red shifted absorption) [23].

In comparison with porphyrin, Zn-metallated complex exhibit emission band around 627 nm and 675 nm, whereas free base exhibit band at 672 nm. Generally, there is a drastic change in the PL spectrum upon metallation, with the appearance of one blue shifted band. It seems clear that the 627 nm band is characteristic of the metallated complex [24a]. ZnPn1 has an important band at 620-630 nm and a shoulder band at 660-690 nm. ZnPn2 and ZnPn3 have main band at 628 nm and minor shoulder at 670-690 nm. The absorption and emission wavelength of P/MP are listed in Table 1. Figs. 2 and 3 show the cyclic voltammograms of P/MP reductions (Table 1) in DMF solvent. The reduction potential at −1.20 V leads to the formation of porphyrin anion radical.

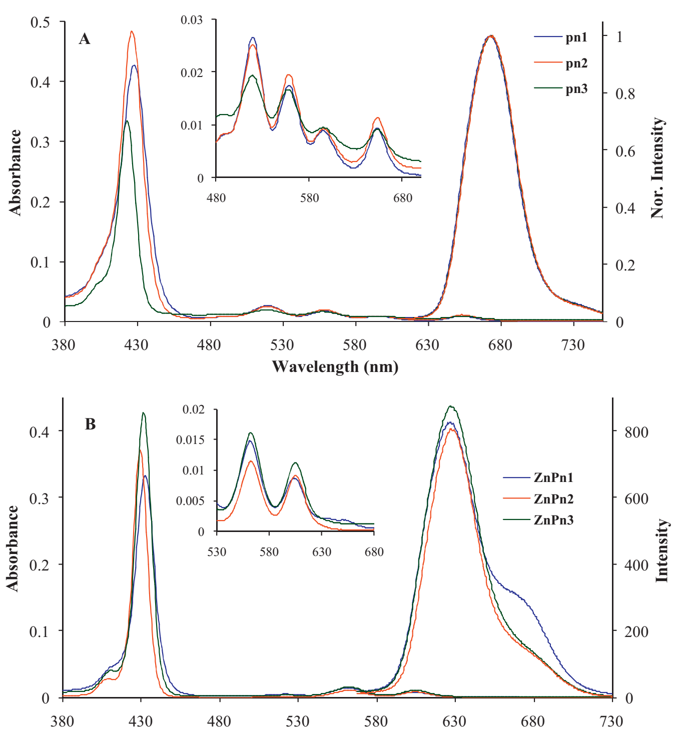

Fig. 1. (A, B) Absorption and emission spectrum of porphyrins and metalloporphyrins in DMF solvent. Insert figure shows expanded Q bands spectrum.

3.2. Ground state interaction

The ground state interaction of TA-CdTe QDs with P/MP is probed through UV–Visible absorbance measurements. Absorption and emission spectrum of QDs observed at 544 nm and 595 nm, respectively. Initially we analyzed the absorption behavior of QDs with 1:1 (QDs:porphyrin) ratio, however we did not observe any significant changes in the absorption behavior. Hence we have used higher concentration of porphyrins relative to QDs as similar to literature reports [24b]. We analyzed the absorption behavior of QDs in different concentrations of porphyrin (1-5 × 10^{-5} M) as displayed in Fig. SI 19. On increasing the concentration of porphyrins there is significant changes in the absorption behavior of QDs. Fig. 4A and B displays the absorption behavior of QDs (1 × 10^{-6} M) in the absence and presence of Pn3 and ZnPn1 at a fixed concentration of (5 × 10^{-5} M). Absorption spectrum of Pn3 shows the intense

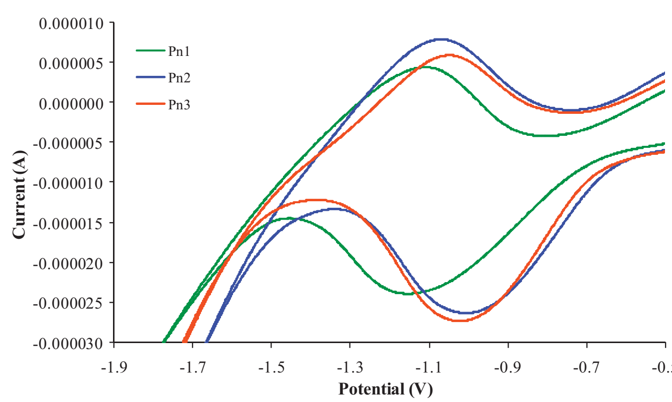

Fig. 2. Cyclic voltammograms of porphyrins.

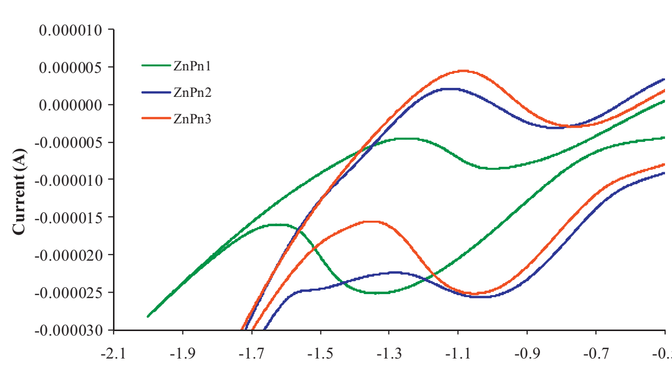

Fig. 3. Cyclic voltammograms of metalloporphyrins.

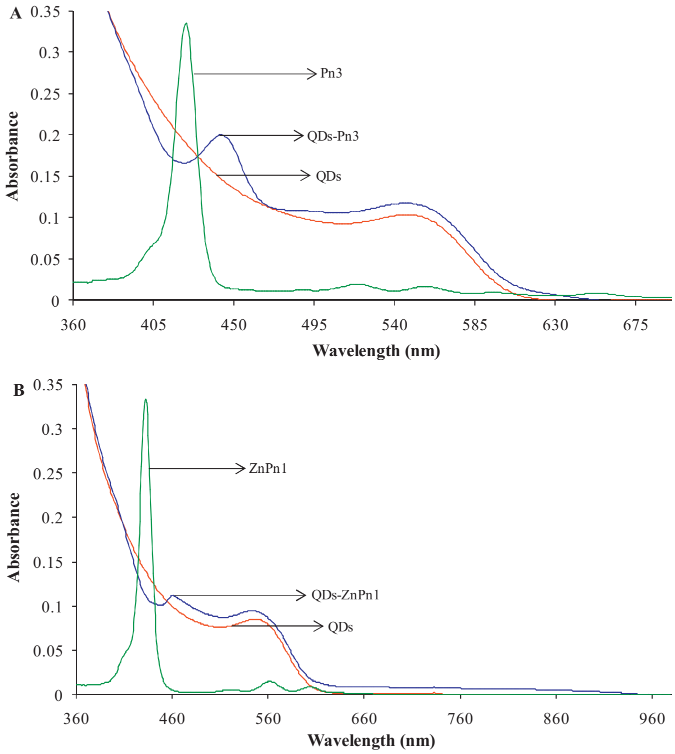

Fig. 4. (A) Absorption spectrum of (i) TA-CdTe QDs (1×10^{-6} M; red line), (ii) Pn3 (5×10^{-5} M; green line), (iii) QDs in the presence of Pn3 (blue line) in water. (B) Absorption spectrum of (i) CdTe QDs (1×10^{-6} M; red line), (ii) ZnPn1 (5×10^{-5}M; green line), (iii) QDs in the presence of ZnPn1 (blue line) in water. (For interpretation of the references to colour in this figure legend, the reader is referred to the web version of this article.)

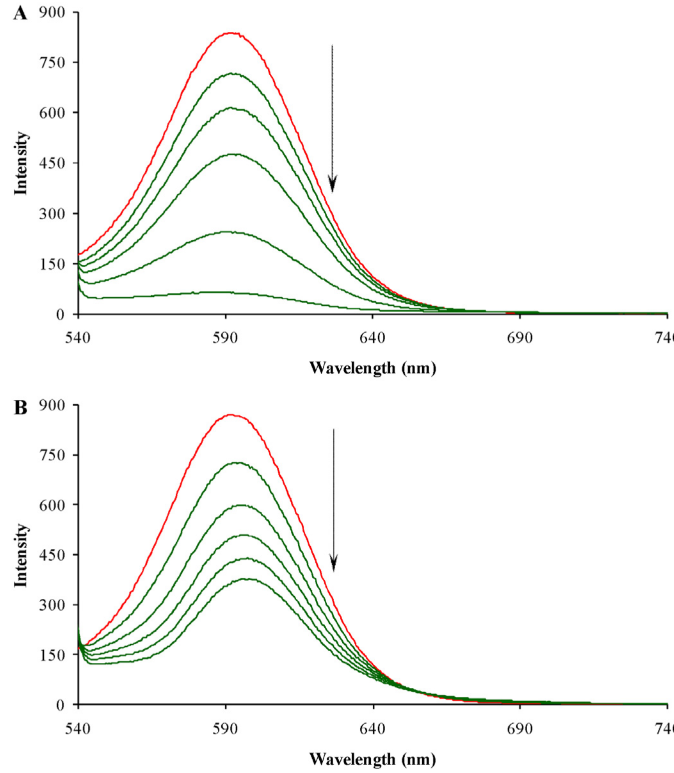

Fig. 5. (A) Emission spectrum of TA-CdTe QDs (1×10^{-6} M; red line) in the absence and presence of Pn3 (0–5×10^{-5} M; green line) in water. The arrow indicates the intensity decrease with increasing concentration of Pn3. (B) Emission spectrum of TA-CdTe QDs (1×10^{-6}M; red line) in the absence and presence of ZnPn1 (0–5×10^{-5} M; green line) in water. The arrow indicates the intensity decrease with increasing concentration of ZnPn1. (For interpretation of the references to colour in this figure legend, the reader is referred to the web version of this article.)

Soret band at 423 nm and 432 nm, respectively. In the presence of Pn3, absorbance of QDs increases, while the soret band of porphyrin was red shifted from 423 to 440 nm. In a similar way, the absorbance of CdTe increases and accompanied with a red shift (432–457 nm) in the presence of ZnPn1. The electronic distribution of porphyrin moiety altered on interaction with QDs which resulted in red shifted absorption behavior. Similar type of red shift absorption behavior has been observed in literature [1]. Similar type of absorption behavior is observed for Pn1, Pn2, ZnPn2, and ZnPn3 (spectra not shown here).

3.3. Excited state interaction

Excited state interactions of P/MP on QDs are investigated by PL measurements. Similar to absorption behavior, Fig. 5A and B displays the spectral change in the emission intensity of QDs with variable concentration of Pn3 and ZnPn1, respectively. The emission intensity of QDs is quenched on increasing the concentration of Pn3 ($0 - 5 \times 10^{-5}$ M). Similar type of quenching behavior has been observed for Pn1 and Pn2. While increasing the concentration of ZnPn1, the emission intensity decreases along with red shift (∼5 nm). The observed red shift reflects the formation of complex between QD and porphyrins in the ground state with the corresponding change of Stokes shift for QD absorption and emission bands. This indicates the formation of complex between QD and porphyrins in the excited state. The other metalloporphyrins also exhibits the similar type of emission behavior (spectra not shown here). The quenching of QDs by P/MP can be described by Stern–Volmer equation.

$$\frac{I_0}{I} = 1 + K_{sv}[Q]$$

where I_0 and I are the emission intensity of QDs in the absence and presence of porphyrins and metalloporphyrins, K_{sv} is the Stern–Volmer constant, Q is quencher concentration. The bimolecular quenching rate constant (k_q) is calculated by using $K_{sv} = k_q.\tau$, where τ is the lifetime of TA-CdTe QDs (11.77 ns). The comparisons of Stern–Volmer plot for the quenching of QDs by P/MP are shown in Fig. 6. A plot between I_0/I vs. [Q], results in straight line for metalloporphyrins. From the plot, the k_q and K_{sv} values are determined (Table 2). The k_q value is found to be higher than the maximum collisional (dynamic) quenching (2×10^{10} M^{-1} s^{-1}). Hence, the PL quenching of QDs is mainly due to complex formation with (i.e., static). In the case of free base porphyrins, an upward Stern–Volmer

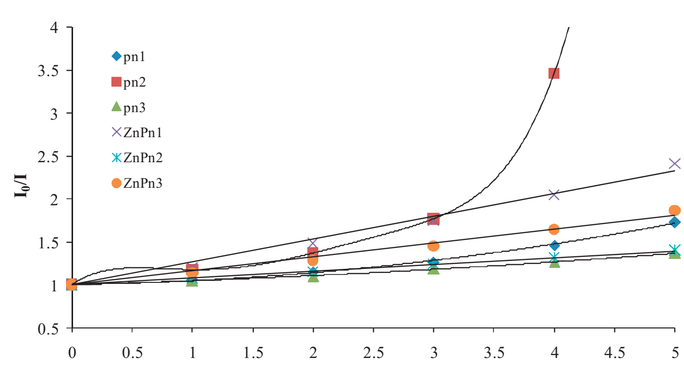

Fig. 6. Comparison of Stern–Volmer plot for QDs with porphyrins and metalloporphyrins. (For interpretation of the references to colour in this figure legend, the reader is referred to the web version of this article.)

Table 2
Stern–Volmer constant (K_{sv}), quenching rate constant (k_q) for metalloporphyrins and binding constant (K) calculated from Benesi and Hildebrand equation, free energy values (ΔG) for P/MP.

P/MP	$K_{sv} \times 10^5$ (M^{-1})	$k_q \times 10^{12}$ ($M^{-1}\,s^{-1}$)	$K \times 10^3$ (M^{-1})	ΔG (eV)
Pn1	–	–	6.93	−0.426
Pn2	–	–	3.22	−0.459
Pn3	–	–	2.35	−0.481
ZnPn1	0.265	2.25	11.666	−0.278
ZnPn2	0.162	1.37	6.976	−0.402
ZnPn3	0.080	0.01	5.806	−0.447

plot is obtained which suggest the occurrence of static quenching along with dynamic quenching [25]. However, a more accurate method like lifetime measurements will provide the clear picture to differentiate the static and dynamic quenching [26].

3.4. TCSPC measurements

Static and dynamic quenching can be clearly distinguished from lifetime measurements. QDs were excited by laser pulse at 375 nm, to measure the decay time of QDs at their maximum emission peak (595 nm). Fig. 7 shows the PL decay curve of TA-CdTe QDs in the absence and presence of Pn1 and ZnPn1. The decay profiles are well fitted with tri-exponential function; $I(t) = \alpha_1 \exp(-t|\tau_1) + \alpha_2 \exp(-t|\tau_2) + \alpha_3 \exp(-t|\tau_3)$. The average decay times are 11.77 ns for 3.21 nm QDs (without pn1). In the presence of pn1, we did not observe any difference in the lifetime of QDs (11.44 ns). Similar behavior is observed for Pn2, Pn3 which confirms the quenching is only due to the complex formation. The decay curve of QDs remains unchanged with high concentration of ZnPn1 (10.88 ns) and other metal porphyrins. Similar behavior obtained for other metalloporphyrins. It clearly reveals that the PL quenching follows static mechanism [27a]. Hence, from the PL measurements, the binding constant for the complex formation can be calculated by using the following equation [27b].

$$\frac{1}{(F^0 - F)} = \frac{1}{(F^0 - F')} + \frac{1}{K(F^0 - F')[Q]}$$

where F^0 is the emission intensity of QDs, F is the observed fluorescence intensity at its maximum, F' is the emission intensity of QDs in the presence of porphyrins/metalloporphyrins. A plot between $1/(F^0 - F)$ vs. $1/[Q]$ gives a straight line (Fig. 8) and the binding constant is calculated from the slope (Table 2). The observed binding affinity decreased in the following order

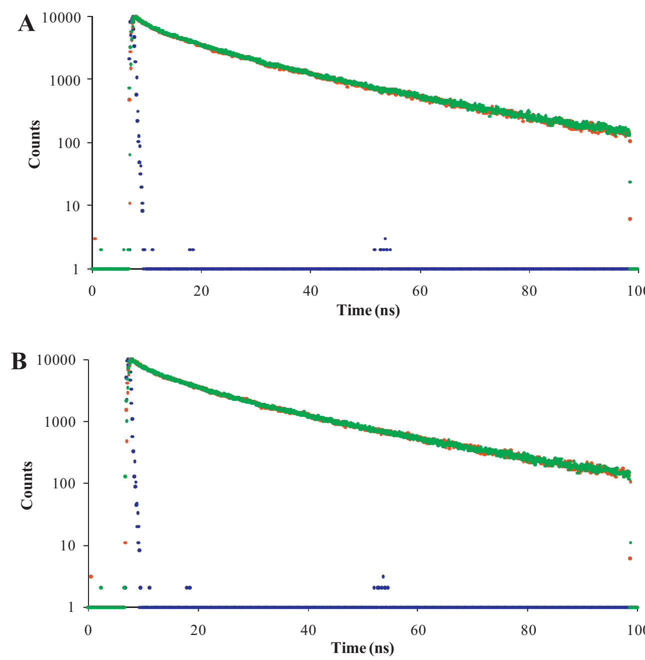

Fig. 7. (A) Lifetime decay curve of TA-CdTe QDs (red color) in the presence of Pn1 (5×10^{-5} M) (green color). (B) Lifetime decay curve of TA-CdTe QDs (red color) in the presence of ZnPn1 (5×10^{-5} M) (green color). (For interpretation of the references to colour in this figure legend, the reader is referred to the web version of this article.)

This illustrates that the insertion of metal in the porphyrins core enhances the binding ability with QDs.

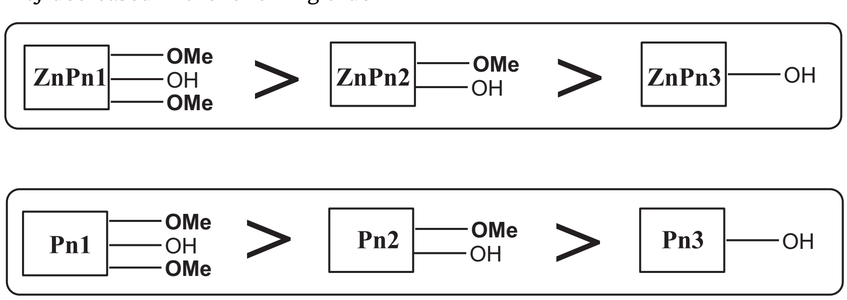

For free base porphyrins, Pn1 have two —OCH3 group and one —OH group which can anchor strongly to the surface of QDs shows higher binding constant, in case of Pn2, one —OCH3 group and one —OH group is present which shows lesser K value than Pn1, while the least binding affinity observed for Pn3 which contains —OH group only. It is clear that on increasing methoxy group the binding constant value increases. Similarly for MP, ZnPn1 which have more methoxy group than ZnPn2, ZnPn3 shows higher K value. While comparing the P/MP, MP has higher binding constant value.

3.5. Possibility of electron transfer process

PL quenching can occur by either energy transfer or electron transfer mechanism. The possibility of energy transfer is less, since the emission spectrum of TA-CdTe QDs is not effectively overlapped with the absorption peaks of Pn1/ZnPn1 is shown in Fig. 9. Energy transfer usually involves the decrease in lifetime of QDs (donor)

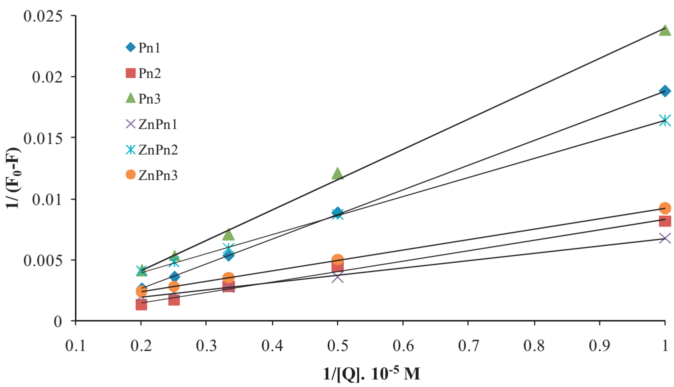

Fig. 8. Comparison of binding constant for QDs with porphyrins and metalloporphyrins.

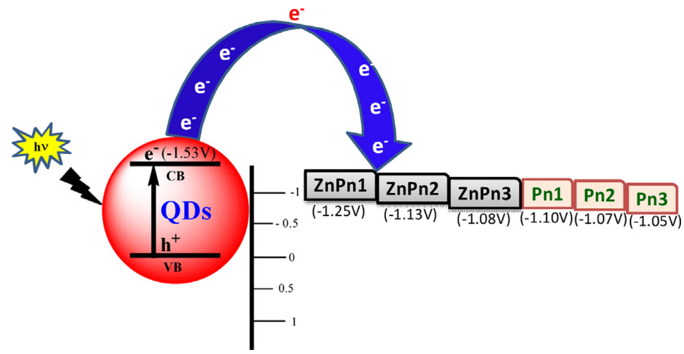

Scheme 4. Energy level diagram.

in the presence of porphyrins (acceptor) as evidenced from literature reports. The unchanged lifetime of QDs in the presence of porphyrins neglects the possibilities of energy transfer from QDs to P/MP [28]. Borczyskowski et al. observations on QDs porphyrin systems reveal that while adding porphyrins to the QDS, the emission intensity of QDs decreases along with the increase in the emission of porphyrin systems which supports the energy transfer from QDs to porphyrin system. Along with FRET mechanism they also proposed the non-FRET mechanism due to the formation of trap states due to ligand removal which results luminescence quenching. While comparing to our system, we did not observed any fluorescence of porphyrins during the addition of porphyrins to the QDs (Fig. 5A and B) and this further supports there is no possibilities of energy transfer role. All these facts supports the energy transfer mechanism is not possible in the systems under study [19]. Hence, electron transfer mechanism might be probable. The possibility of electron transfer mechanism is analyzed through energy level diagram, Rehm–Weller equation and laser flash photolysis. For electron transfer to occur, the conduction band potential of QDs should be more negative than the reduction potential of P/MP. The conduction band potential of QDs is −1.53 V vs Ag/AgCl which is more negative than the reduction potential of P/MP (Table 1). Hence, the transfer of electrons from the QDs to P/MP is feasible (Scheme 4). Further we analyzed the quenching of porphyrins by QDs (reverse manner). Pn1 is excited at 428 nm and the emission is monitored at 672 nm. As seen from the figure SI 20, the observed emission of QDs reveals that the QDs also excited at the excitation wavelength of porphyrins. This makes more complicated for accurate analysis. When we look over the potential levels of QDs and porphyrin, it is clear that the excited QDs can transfer the electron to the porphyrins under study, and not from excited porphyrin to QDs. Further there is minimal overlap between the porphyrin emission and QD absorption neglects the possibilities of energy transfer between them. The important parameter for applying these systems in solar energy conversion is the possibility of electron transfer. Hence we excited the QDs and studied their electron transfer properties to the porphyrin systems and not vice versa. The thermodynamic feasibility of the excited state electron transfer reactions is calculated through Rehm–Weller equation [29].

$$\Delta G_{et} = E_{1/2}^{(\mathrm{oxi})} - E_{1/2}^{(\mathrm{red})} - E^{*}$$

where ΔG_{et} is change in free energy, $E_{1/2}^{(\mathrm{oxi})}$ is the conduction band potential of TA-CdTe QDs (donor). $E_{1/2}^{(\mathrm{red})}$ is the reduction potential of porphyrins/metalloporphyrins (acceptors), E^{*} is the excited state energy of TA-CdTe QDs (2.16 eV, calculated from the cross-section of absorption and PL spectra). The change in free energy values is found to be negative and is listed in Table 2. The observed negative value indicates the electron transfer processes is thermodynamically feasible [30]. Hence, the P/MP has the ability to capture photogenerated electrons from QDs which is supported by energy level diagram and Rehm–Weller equation. Further, the electron transfer process is analyzed through nanosecond laser flash photolysis.

3.6. Nanosecond transient absorption studies

The transient absorption spectrum of QDs, ZnPn1 and QDs-ZnPn1 (at 0.1 μs) in degassed aqueous medium is recorded after a nanosecond laser flash photolysis using 532 nm laser pulse as the excitation source. In Fig. 10, the negative absorption peak of QDs (bleach) is observed from 520 to 680 nm with peak maxima at 590 nm, with slight shift corresponds to ground state absorption

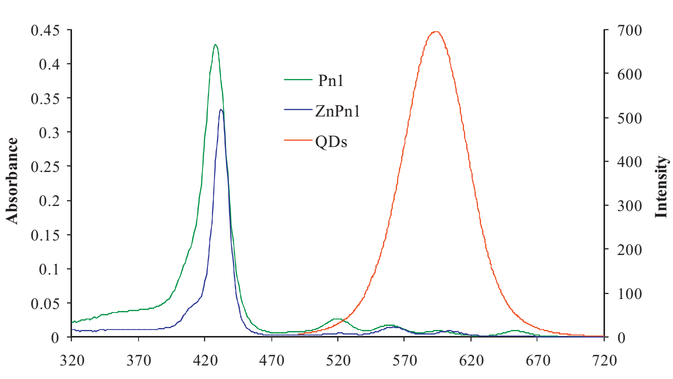

Fig. 9. Emission spectrum of QDs and absorption spectrum of Pn1 and ZnPn1.

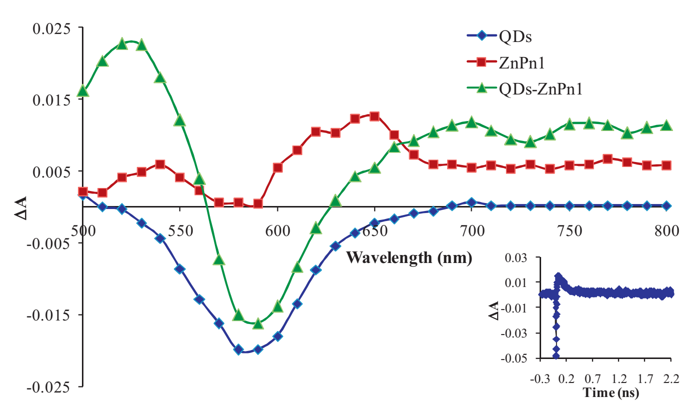

Fig. 10. Transient absorption spectra recorded after a laser pulse excitation of QDs-ZnPn1 solution in aqueous medium. Inset shows the kinetic trace observed at 700 nm.

(547 nm). For ZnPn1, the metal Q (1, 0) band was appeared at 540 nm and stimulated emission band at 620-650 nm. In the presence of ZnPn1, transient absorption spectrum of QDs shows a recovery of ground state bleach and a stimulated emission peak (ZnPn1) is completely disappear and forms a new absorption band in the range of 670-800 nm. This peak is clearly observed after a laser flash, can be assigned to ZnPn1 anion radical which indicates that excitions dissociate by electron transfer from QDs to ZnPn1. Similar type of MP anion radical is found in literature [31]. Photoinduced electron transfer proceeds to yield the charge separated state as given in following equation.

$$\mathrm{CdTe} \xrightarrow{h\nu} \mathrm{CdTe(e^-)} + \mathrm{CdTe(h^+)}$$
$$\mathrm{CdTe(e^-)} + \mathrm{ZnPn1} \rightarrow \mathrm{ZnPn1}^{\bullet -}$$

Inset of Fig. 10 shows that the kinetic decay trace was monitored at 700 nm. The lifetime of ZnPn1 anion radical is evaluated to be 11 ns can be fitted by bi-exponential decay function. Similar observation is addressed in the literature [26]. These results support the evidence of electron transfer from QDs to ZnPn1.

4. Conclusion

TA-CdTe QDs, free base porphyrins and metalloporphyrins were successfully synthesized and characterized by ^{1}H and ^{13}C NMR, mass, IR, cyclic voltammetry and steady state absorbance and PL measurements. The interaction between QDs and P/MP was investigated by various spectroscopic techniques. Ground state complex formation was observed through absorption measurements. Static type of PL quenching has been confirmed through lifetime measurements. From the PL quenching data, it was inferred that on increasing the $-OCH_3$ groups in P/MP, its binding affinity with QDs increases. Further, the insertion of metal increases the binding affinity with QDs as compared to free base porphyrins. The conduction band potential of QDs was more feasible to donate electrons to the reduction potential of P/MP. ZnPn1 anion radical was appeared in the range of 670−800 nm in transient absorption measurements reveals electron transfer from QDs to ZnPn1. Surface passivation of QDS with organic molecules is currently an important topic for increasing the solar energy conversion efficiency. In this scenario we believe that the observed binding behavior, feasible potential values, electron transfer process will provide prolific information for the usage of QDs–porphyrins system in future designing of solar cells. Currently we are investigating the potential usage of these systems in solar energy conversion in our laboratory.

Acknowledgements

R.R. thanks DST (Ref. No. SR/S1/PC-12/2011,DT: 20.09.2011) for the Project. S.J. (Ref. No: 039680/E15/2011 Dt: 17.02.2011) and G.P. (Ref. No: 07722/E15/2012, Dt: 28.03.2012) thank UGC-BSR (RFSMS) for the Fellowship. Authors also thank UGC/DST-FIST for NMR and IR facilities in the School of Chemistry, Bharathidasan University. We are thankful to Prof. P. Ramamurthy, Director, NCUFP, University of Madras, Chennai for lifetime and transient measurements.

Appendix A. Supplementary data

Supplementary material related to this article can be found, in the online version, at http://dx.doi.org/10.1016/j.jphotochem.2013.11.018.

References

[1] J.J.H. Pijpers, R. Koole, W.H. Evers, A.J. Houtepen, S. Boehme, C. de Mello Donega, et al., Spectroscopic studies of electron injection in quantum dot sensitized mesoporous oxide films, Journal of Physical Chemistry C 114 (2010) 18866.
[2] V.L. Colvin, M.C. Schlamp, A.P. Allvisatos, Light-emitting diodes made from cadmium selenide nanocrystals and a semiconducting polymer, Nature 370 (1994) 354.
[3] M.G. Calvete, Y. Yang, M. Hanack, Porphyrins and phthalocyanines as materials for optical limiting, Synthetic Metals 141 (2004) 231.
[4] V.I. Klimov, A.A. Mikhailovsky, S. Xu, A. Malko, J.A. Hollingsworth, C.A. Leatherdale, et al., Optical gain and stimulated emission in nanocrystal quantum dots, Science 290 (2000) 314.
[5] (a) M. Bruchez Jr., M. Moronne, P. Gin, S. Weiss, A.P. Alivisatos, Semiconductor nanocrystals as fluorescent biological labels, Science 281 (1998) 2013;
(b) W.C.W. Chan, S. Nile, Quantum dot bioconjugates for ultrasensitive nonisotopic detection, Science 281 (1998) 2016.
[6] I.J. Macdonald, T.J. Dougherty, Basic principles of photodynamic therapy, Journal of Porphyrins and Phthalocyanines 5 (2001) 105.
[7] G.S. Paul, J.H. Kim, M.S. Kim, K. Do, J. Ko, J.S. Yu, Different hierarchical nanostructured carbons as counter electrodes for CdS quantum dot solar cells, Applied Material and Interfaces 4 (2012) 375.
[8] T.L. Li, Y.L. Lee, H. Teng, High-performance quantum dot-sensitized solar cells based on sensitization with $CuInS_2$ quantum dots/CdS heterostructure, Energy and Environmental Sciences 5 (2012) 5315.
[9] (a) M.C. Beard, Multiple exciton generation in semiconductor quantum dots, Journal of Physical Chemistry Letters 2 (2011) 1282;
(b) A. Pandey, P. Guyot-Sionnest, Hot electron extraction from colloidal quantum dots, Journal of Physical Chemistry Letters 1 (2010) 45.
[10] E.A. Viktorov, M. Paul Mandel Kuntz, G. Fiol, D. Bimberg, A.G. Vladimirov, M. Wolfrum, Stability of the mode-locked regime in quantum dot lasers, Applied Physics Letters 91 (2007) 231116.
[11] G. Hodes, Comparison of dye- and semiconductor-sensitized porous nanocrystalline liquid junction solar cells, Journal of Physical Chemistry C 112 (2008) 17778.
[12] Y.L. Lee, B.M. Huang, H.T. Chin, Highly efficient CdSe-sensitized TiO_2 photoelectrode for quantum-dot-sensitized solar cell applications, Chemistry of Materials 20 (2008) 6903.
[13] M. Shalom, S. Dor, S. Ruhle, L. Grinis, A. Zaban, Core/CdS quantum dot/shell mesoporous solar cells with improved stability and efficiency using an amorphous TiO_2 coating, Journal of Physical Chemistry C 113 (2009) 3895.
[14] (a) M. Sykora, M.A. Petruska, J.A. Acevedo, I. Bezel, T.J. Meyer, V.I. Klimov, Photoinduced charge transfer between CdSe nanocrystal quantum dots and Ru–polypyridine complexes, Journal of the American Chemical Society 128 (2006) 9984;
(b) E.I. Zenkevich, C. Von Borczyskowski, Photoinduced relaxation processes in self-assembled nanostructures: multiporphyrin complexes and composites "CdSe/ZnS quantum dot–porphyrin, Macroheterocycles 2 (2009) 206;
(c) E. Zenkevich, F. Cichos, A. Shulga, E.P. Petrov, T. Blaudeck, C. von Borczyskowski, Nanoassemblies, designed from semiconductor quantum dots and molecular arrays, Journal of Physical Chemistry B 109 (2005) 8679;
(d) P.M. Keane, S.A. Gallagher, L.M. Magno, M.J. Leising, I.P. Clark, G.M. Greetham, et al., Photophysical studies of CdTe quantum dots in the presence of a zinc cationic porphyrins, Dalton Transactions 41 (2012) 13159.
[15] (a) A. Hagfeldt, M. Grätzel, Molecular photovoltaics, Accounts of Chemical Research 33 (2000) 269;
(b) D.J. Norris, M.G. Bawendi, L.E. Brus, J. Jortner, M. Ratner (Eds.), Molecular Electronics, Blackwell Science, Oxford, 2002, p. 281.
[16] K. Kalyanasundaram, M. Neumann-Spallart, Photophysical and redox properties of water-soluble porphyrins in aqueous media, Journal of Physical Chemistry 86 (1982) 5163.
[17] (a) J. Huang, D. Stockwell, Z. Huang, D.L. Mohler, T. Lian, Photoinduced ultrafast electron transfer from CdSe quantum dots to Re-bipyridyl complexes, Journal of the American Chemical Society 130 (2008) 5632;
(b) A. Boulesbaa, A. Issac, D. Stockwell, Z. Huang, J. Huang, J. Guo, et al., Ultrafast charge separation at CdS quantum dot/Rhodamine B molecule interface, Journal of the American Chemical Society 129 (2007) 15132.
[18] (a) S. Issac, T. Jin, Lian, Intermittent electron transfer activity from single CdSe/ZnS quantum dots, Journal of the American Chemical Society 130 (2008) 11280;
(b) S. Mandal, M. Rahaman, S. Sadhu, S.K. Nayak, A. Patra, Fluorescence switching of quantum dot in quantum dot–porphyrin–cucurbit [7] uril assemblies, Journal of Physical Chemistry C 117 (2013) 3069.
[19] (a) T. Blaudeck, E.I. Zenkevich, M.A. Mottaleb, K. Szwaykowska, D. Kowerko, F. Cichos, C. von Borczyskowski, Formation principles and ligand dynamics of nanoassemblies of cdse quantum dots and functionalised dye molecules, ChemPhysChem 13 (2012) 959;
(b) E. Zenkevich, F. Cichos, A. Shulga, E.P. Petrov, T. Blaudeck, C. von Borczyskowski, Nanoassemblies designed from semiconductor quantum dots and molecular arrays, Journal of Physical Chemistry B 109 (2005) 8679;
(c) E.I. Zenkevich, T. Blaudeck, A. Milekhin, C. von Borczyskowski, Size-Dependent non-FRET photoluminescence quenching in nanocomposites based on semiconductor quantum dots CdSe/ZnS and functionalized porphyrin ligands, International Journal of Spectroscopy (2012), http://dx.doi.org/10.1155/2012/971791.
[20] M. Asha Jhonsi, R. Renganathan, Investigations on the photoinduced interaction of water soluble thioglycolic acid (TGA) capped CdTe quantum dots with certain porphyrins, Journal of Colloid and Interface Sciences 344 (2010) 596.
[21] X. Guo, W. An, S. Shuang, F. Cheng, C. Dong, Study on spectroscopic characterization of meso-tetrakis (4-hydroxyphenyl) porphyrin (THPP) in β-cyclodextrin

and its derivatives, Journal of Photochemistry and Photobiology: A Chemistry 173 (2005) 258.

[22] X. Liu, J. Liu, K. Jin, X. Yang, Q. Peng, L. Suna, Synthesis, characterization and some properties of amide-linked porphyrin–ruthenium(II) tris(bipyridine) complexes, Tetrahedron 61 (2005) 5655.

[23] (a) W.N. Yen, S.S. Lo, M.C. Kuo, C.L. Mai, G.H. Lee, S.M. Peng, C.Y. Yeh, Synthesis, structure, and optical and electrochemical properties of star-shaped porphyrin-triarylamine conjugates, Organic Letters 8 (2006) 4239;
(b) X. Qiu, R. Lu, H. Zhou, X. Zhang, T. Xu, X. Liu, Y. Zhao, Synthesis of phenothiazine-functionalized porphyrins with high fluorescent quantum yields, Tetrahedron Letter 49 (2008) 7446.

[24] (a) E.F. Cosma, C. Enachea, I. Armeanua, G.F. Cosma, Comparative investigations of the absorption and fluorescence spectra of tetrapyridylporphyrine and Zn(II) tetrapyridylporphyrine, Digest Journal of Nanomaterials and Biostructures 2 (2007) 175;
(b) M.L. Christopher, K. Elizabeth, G.B. Moungi, G.N. Daniel, Two-photon oxygen sensing with quantum dot–porphyrin conjugates, Inorganic Chemistry 52 (2013) 10394.

[25] P.J. Goutam, D.K. Singh, P.K. Iyer, Photoluminescence quenching of poly(3-hexylthiophene) by carbon nanotubes, Journal of Physical Chemistry C 116 (2012) 8196.

[26] S.C. Cui, T. Tachikawa, M. Fujitsuka, T. Majima, Interfacial electron transfer dynamics in a single CdTe quantum dot–pyromellitimide conjugate, Journal of Physical Chemistry C 112 (2008) 19625.

[27] (a) T.K. Mukherjee, P.P. Mishra, A. Datta, Photoinduced electron transfer from chlorin p6 to methyl viologen in aqueous micelles, Chemical Physical Letters 407 (2005) 119;
(b) P.V. Kamat, B. Patrick, Photophysics and photochemistry of quantized zinc oxide colloids, Journal of Physical Chemistry 96 (1992) 6829.

[28] X. Zhang, Z. Liu, L. Ma, M. Hossu, W. Chen, Interaction of porphyrins with CdTe quantum dots, Nanotechnology 22 (2011) 195501.

[29] G.J. Kavarnos, N.J. Turro, Photosensitization by reversible electron transfer: theories, experimental evidence, and examples, Chemical Reviews 86 (1986) 401.

[30] S. Nath, H. Pal, D.K. Palit, A.V. Sapre, J.P. Mittal, Steady-state and time-resolved studies on photoinduced interaction of phenothiazine and 10-methylphenothiazine with chloroalkane, Journal of Physical Chemistry A 102 (1998) 5822.

[31] K. Kalayanasundaram, Mechanism of photoreduction of water-soluble palladium and zinc porphyrins, Journal of Photochemistry and Photobiology: A Chemistry 42 (1988) 87.